Title:

Spatiotemporal evolution of temperature extremes across India's agro-climatic zones (1951–2025)

Running title:

Temperature Extremes across India's Agro-Climatic Zones

Ashutosh Kumar Misra[1], Sudhir Kumar Mishra[2], Santosha Rathod[2], Kripan Ghosh[3], Asha Latwal[1], M R Deo[1], K G Kanade[1]

[1]Agricultural Meteorology Division, India Meteorological Department, Shivajinagar, Pune–411005, Maharashtra, India

[2]ICAR–National Institute of Abiotic Stress Management, Baramati–413102, Maharashtra, India

[3]Regional Meteorological Centre, India Meteorological Department, Guwahati-781015, Assam, India

*Correspondence: Ashutosh Kumar Misra (dr.ashutosh.misra@imd.gov.in); ORCID: 0000-0002-9252-1502

Peer review status:
This is a a non-peer reviewed preprint submitted to EarthArXiv. The original manuscript has been submitted to the International Journal of Climatology

Abstract

Long-term changes in temperature extremes are a robust signature of anthropogenic climate change, yet their spatial structure across India's agro-climatic zones (ACZs) remains insufficiently resolved at policy scales. Here, we quantify changes in temperature extremes across 14 mainland ACZs during 1951–2025 using the India Meteorological Department 1°×1° gridded daily dataset. We compute 22 indices, including 11 ETCCDI metrics, 7 India-specific thresholds, and 4 crop-specific growing degree day (GDD) indices, and assess trends using the Mann–Kendall test with trend-free pre-whitening and Sen's slope estimator. Tropical Nights (TR20; Tmin ≥ 20 °C) exhibit the most spatially coherent increase, with significant trends in 10 of 12 Tier A/B zones, peaking in the Western Dry Region (ACZ-14; +3.182 days decade^{-1}; $p < 0.05$). Warm-day frequency (TX90p) increases significantly in 9 zones, with strongest trends in the Southern Plateau (+2.962% decade^{-1}), East Coast Plains (+2.940% decade^{-1}), and West Coast Plains and Ghats (+2.917% decade^{-1}). Diurnal temperature range declines in 8 zones, indicating faster warming of minimum than maximum temperatures across Gangetic, arid, and interior plateau regions, while coastal and southern plateau zones show daytime-dominant warming. Seasonal thermal accumulation intensifies, with significant increases in rabi wheat GDD in the Trans-Gangetic Plain (+11.130 GDD decade^{-1}) and Gujarat Plains (+21.625 GDD decade^{-1}). Temporal analysis identifies 2001–2025 as the warmest 25-year period in the 1951–2025 record across most ACZs. These results provide the first comprehensive ACZ-level ETCCDI characterisation of India's 75-year thermal extreme record, revealing spatially heterogeneous warming with pronounced nocturnal intensification across the Gangetic and arid zones and daytime-dominant warming in coastal and southern plateau zones, with direct relevance for agricultural adaptation planning.

Keywords: Temperature extremes; ETCCDI; agro-climatic zones (ACZ); tropical nights; diurnal temperature range; crop thermal stress

1. Introduction

The progressive intensification of temperature extremes is among the most documented manifestations of anthropogenic climate change. Globally, warm days, warm nights, and heatwave events have intensified since the mid-twentieth century while cold extremes have declined in frequency and severity (IPCC, 2021; Alexander et al., 2006; Donat et al., 2013; Perkins-Kirkpatrick and Gibson, 2017), and attribution analyses have established a dominant anthropogenic contribution to these changes through greenhouse gas forcing (Fischer and Knutti, 2015). Perkins-Kirkpatrick and Lewis (2020) documented a tripling of global heatwave days between 1950 and 2017, and Raymond et al. (2020) demonstrated that heat-humidity combinations dangerous to human physiology are emerging across tropical and subtropical agricultural landscapes at rates that outpace autonomous adaptive capacity. For food systems serving billions of smallholder farmers, the spatial and temporal characterization of these changes is no longer merely academic but a prerequisite for evidence-based adaptation policy.

India encapsulates this challenge at exceptional scale. With a population exceeding 1.4 billion, an agricultural sector contributing 17–18% of GDP and employing nearly 45% of the workforce (Ministry of Agriculture and Farmers Welfare, 2023), and a physiographic envelope spanning equatorial coastlines, tropical semi-arid plains, hyper-arid deserts, and Himalayan highlands, the country encompasses perhaps the broadest range of agro-climatic environments on Earth. The Indian monsoon introduces strong seasonal modulation of temperature variability that interacts non-linearly with the secular anthropogenic warming trend, generating regionally heterogeneous responses that spatially aggregated national analyses cannot resolve (Rohini et al., 2019; Dash and Mamgain, 2011). Crop-specific heat damage operates through well-defined

physiological thresholds: wheat temperatures exceeding 30°C during grain filling suppress starch synthase activity and reduce kernel weight, with each additional degree of warming compressing the grain-filling period by two to three days (Misra et al., 2019a; Pal et al., 2008); night-time temperatures above 27°C impair rice pollen viability and elevate spikelet sterility during the reproductive stage; and sustained cotton maxima above 40°C induce boll shedding and fibre quality deterioration (Ban et al., 2013). Zone-specific thermal trajectories are therefore essential inputs for crop model calibration, variety development, and sowing calendar design.

Existing analyses of Indian temperature extremes have established a warming baseline but leave important gaps. A centennial warming rate of approximately 0.52°C per 100 years was documented for 1901–2007 (Kothawale et al., 2010), while spatially heterogeneous ETCCDI trends across South Asia—most pronounced in minimum temperatures over the Indo-Gangetic Plain—were reported by Revadekar et al. (2012). Rohini et al. (2016, 2019) linked intensifying heatwave frequency to anomalous atmospheric circulation and CMIP5 projections, and Srivastava et al. (2009) developed the IMD high-resolution gridded dataset underpinning the present analysis. However, most prior studies employ spatial aggregations misaligned with the operationally relevant agro-climatic zone (ACZ) structure, use indices unadapted to Indian thermal conditions, or predate the record-warm years of 2015–2024 (WMO, 2024). No existing study covers the full 1951–2025 period at the ACZ level, meaning the globally warmest decade has never been characterised within India's operational agricultural planning framework. The question of daytime versus night-time warming asymmetry—with its direct implications for crop respiration balance and livestock thermoregulation—has similarly received little systematic quantification across the full 14-zone mainland domain.

The ICAR and Planning Commission of India jointly delineated 15 ACZs on the basis of soil type, rainfall seasonality, temperature regime, and crop-growing period length (ICAR, 1989; Planning Commission, 1989). These zones serve as the operational framework for variety recommendation, input-use guidelines, and extension advisories, making them the most policy-relevant spatial unit for communicating climate impacts to agricultural planners. The ETCCDI standardised suite of temperature extreme indices, computed from daily maximum and minimum observations and implemented in R via the climdex.pcic package (Peterson et al., 2001; Alexander et al., 2006; Zhang et al., 2005, 2011; Bronaugh, 2020), provides the methodological backbone. One critical adaptation for Indian conditions replaces the standard Summer Days index (Tmax > 25°C)—a threshold exceeded on the majority of days across most zones and therefore lacking discriminating power—with a 35°C threshold (SU35) consistent with WMO Climpact v2 specifications and Indian agronomic benchmarks (WMO, 2023).

This study delivers a spatiotemporally resolved analysis of 22 temperature extreme indices across India's 14 mainland ACZs for 1951–2025, with specific focus on: (i) the spatial distribution and temporal evolution of thermal extremes; (ii) daytime versus night-time warming asymmetry; (iii) crop-specific seasonal GDD trends using field-validated base temperatures; (iv) warming acceleration assessed through 25-year block comparisons; and (v) agronomic implications for India's diverse agricultural systems. The results constitute the most spatially resolved, zone-specific thermal evidence base currently available for adaptive agricultural planning in India.

2. Datasets and Methods

2.1 Study Domain and Agro-Climatic Zone (ACZ) Framework

The study domain encompasses the 14 mainland ACZs of India as delineated by ICAR (1989) and the Planning Commission (1989), extending from approximately 8°N to 37°N latitude and 68°E to 97°E longitude (Figure 1). These zones span the complete spectrum of Indian agro-

ecological environments: the Himalayan zones (ACZ-1, ACZ-2), the Gangetic alluvial plains (ACZ-3 to ACZ-6), the interior plateau and hill regions (ACZ-7 to ACZ-10), the coastal zones (ACZ-11, ACZ-12), and the arid/semi-arid western zones (ACZ-13, ACZ-14). The Island Region (ACZ-15, Andaman & Nicobar Islands and Lakshadweep) was excluded because no 1°×1° IMD grid centroid falls within its polygon boundaries and the gridded product was designed for the continental landmass and does not extend to these island territories (Srivastava et al., 2009). The ACZ shapefile was obtained from the Open Government Data Platform India (OGD, 2022), standardized to the World Geodetic System 1984 (WGS84) coordinate reference system, and subjected to geometric validation to resolve self-intersecting polygon artifacts using the sf package (Pebesma, 2018) in R. Detailed information on these ACZs, along with the number of 1°×1° grid cells assigned to each ACZ following spatial intersection, is provided in Table 1; total inland coverage across the 14 zones was approximately 307 grid cells.

Figure 1: Spatial distribution of India's 14 mainland agro-climatic zones as characterized by ICAR/Planning Commission. Source: OGD Platform India (2022).

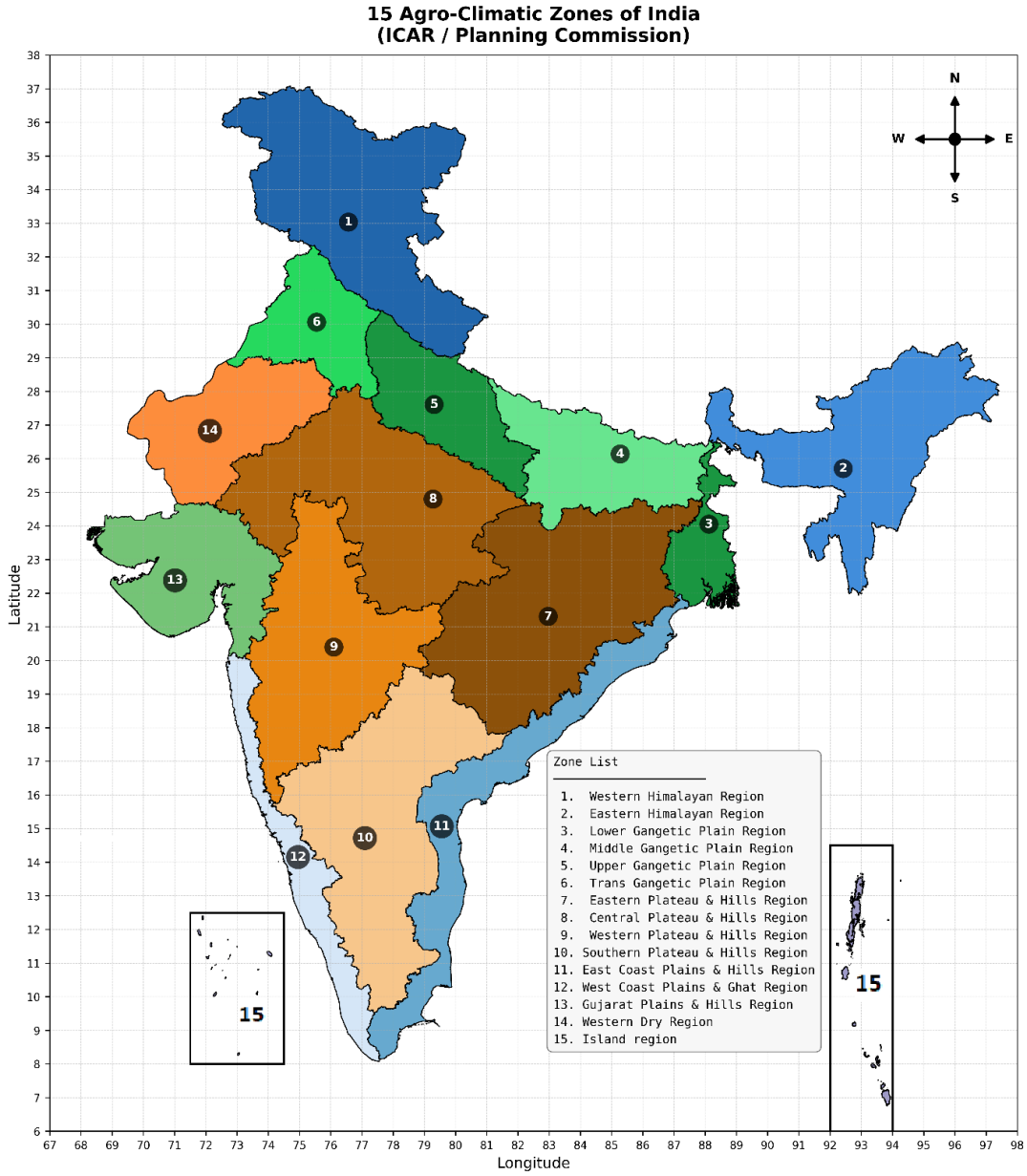

Table 1. Agro-climatic zones (ACZs) of India analysed in this study, showing tier classification, Data Availability period, number of 1°×1° IMD grid cells, dominant crop system, and prevailing climate type as per ICAR/Planning Commission shapefile. ACZ-15 (Island Region) excluded from all analyses; see Section 2.1. Grid-cell counts correspond to intersections with the IMD 1° × 1° gridded temperature dataset.

ACZ No.	Agro-climatic zones	Tier	Data Availability Period	Cells	Dominant crops	Climate type
1	W. Himalayan Region	C	1969–2025	~8	Apple, wheat, barley, saffron	Temperate–Alpine
2	E. Himalayan Region	C	1969–2025	~6	Tea, rice, jhum crops	Humid Temperate
3	Lower Gangetic Plain	A	1951–2025	~18	Rice, jute, mustard	Humid Subtropical
4	Middle Gangetic Plain	A	1951–2025	~22	Wheat–rice, sugarcane, maize	Humid Subtropical
5	Upper Gangetic Plain	A	1951–2025	~12	Wheat–rice, potato, mustard	Semi-arid Subtropical
6	Trans-Gangetic Plain	A	1951–2025	~10	Wheat–rice, cotton, oilseeds	Semi-arid
7	Eastern Plateau & Hills	B	1965–2025	~28	Millets, pulses, oilseeds	Semi-arid Tropical
8	Central Plateau & Hills	A	1951–2025	~38	Soybean, pulses, mustard	Semi-arid Tropical
9	Western Plateau & Hills	A	1951–2025	~32	Cotton, grapes, sorghum	Semi-arid Tropical
10	Southern Plateau & Hills	A	1951–2025	~35	Millets, groundnut, poultry	Semi-arid Tropical
11	East Coast Plains & Hills	A	1951–2025	~20	Rice, coconut, fisheries	Tropical Humid
12	West Coast Plains & Ghats	B	1961–2025	~15	Coconut, spices, rubber, coffee	Tropical Humid
13	Gujarat Plains & Hills	A	1951–2025	~28	Cotton, groundnut, dairy	Arid–Semi-arid
14	Western Dry Region	B	1965–2025	~35	Pearl millet, cluster bean	Arid (Thar Desert)

2.2 Temperature Data and Quality Control

Daily gridded maximum temperature (Tmax) and minimum temperature (Tmin) for 1 January 1951 to 31 December 2025 were sourced from the India Meteorological Department (IMD).

The dataset is produced at 1°×1° spatial resolution spanning 6.5°N–38.5°N and 66.5°E–100.5°E using the modified Shepard's interpolation algorithm applied to a quality-controlled network of surface observatories, and has been widely used in Indian agrometeorological research (Srivastava et al., 2009; Kashyapi et al., 2010). The 1° × 1° IMD gridded temperature dataset was selected because it provides the longest continuous daily record available for India (1951–present), which is essential for robust multi-decadal trend detection in climate extremes. Higher-resolution IMD temperature datasets (e.g., 0.5° × 0.5°) are available only for shorter and more recent periods and therefore cannot support a consistent analysis over the full 75-year study period.

A three-stage quality control (QC) protocol was applied prior to index computation. Missing-value flags (99.9°C) were converted to NA. Physical plausibility checks removed values outside −5 to 55°C for Tmax and −30 to 40°C for Tmin. Internal consistency checks invalidated any day on which Tmin exceeded Tmax. Isolated gaps were filled by linear interpolation using the zoo package (Zeileis and Grothendieck, 2005), with zone-specific maximum gap caps: 7 days for most zones, 15 days for the sparse ACZ-7 and ACZ-14 networks, and 30 days for the Himalayan zones (ACZ-1 and ACZ-2) where multi-week observation gaps are documented in the early instrumental record. A year was considered valid for a grid cell if daily data completeness exceeded 70%, following Zhang et al. (2011). Zone-mean daily temperatures were computed as cosine-latitude-weighted averages across all constituent grid cells (Jones and Hulme, 1996). Zone-mean indices were computed only for years in which at least 60% of the zone's grid cells met the annual completeness threshold, following Donat et al. (2013). All analyses were conducted in R version 4.3 (R Core Team, 2023), using data.table (Dowle and Srinivasan, 2023), lubridate (Grolemund and Wickham, 2011), sf (Pebesma, 2018), Kendall (McLeod, 2022), trend (Pohlert, 2023), climdex.pcic (Zhang et al., 2005; Bronaugh, 2020), zoo (Zeileis and Grothendieck, 2005), and openxlsx (Schauberger and Walker, 2023).

2.3 Three-Tier Analytical Framework

A three-tier framework was adopted to account for spatial heterogeneity in data quality. Tier A comprises nine zones (ACZ-3, 4, 5, 6, 8, 9, 10, 11, 13) with full 1951–2025 analysis and all 22 indices. Tier B comprises three zones with truncated start dates corresponding to documented IMD observatory network expansion: ACZ-7 and ACZ-14 from 1965, ACZ-12 from 1961. Tier C comprises the two Himalayan zones (ACZ-1, ACZ-2) analysed from 1969 with a restricted index set (TXx, TNn, TX90p, TN90p, DTR, GDD_C1, GDD_C2, CDD24, HDD18), excluding spell-duration indices sensitive to data gaps. Within the Himalayan zones, single 1°×1° cells span elevation ranges exceeding 3,000 m, making interpolated values unrepresentative of high-altitude terrain; Tier C results are therefore presented as indicative due to the relatively sparse observational network in high-elevation regions during the early instrumental period, which is also reflected in the gridded IMD dataset.

2.4 ETCCDI Temperature Extreme Indices

Twenty-two temperature extreme indices were computed following the climdex.pcic R package (Zhang et al., 2005; Bronaugh, 2020) and the specifications of Alexander et al. (2006) and Zhang et al. (2011). The full index inventory is given in Table 2. Calendar-day 10th and 90th percentiles for TX90p, TX10p, TN90p, and TN10p were derived using a 5-day moving window centred on each calendar day, pooled across all years of the 1961–1990 WMO reference period (≈150 values per day), strictly following the Zhang et al. (2011) methodology. Hot Days (SU35; Tmax $\geq$ 35°C) replaces the standard ETCCDI SU25 as the primary India-relevant warm-day threshold, consistent with the WMO Climpact v2 framework; SU25 is retained for global comparability. The Heatwave Days index (HWD) follows IMD operational criteria: Tmax $\geq$ 40°C for plains zones, Tmax $\geq$ 30°C for Himalayan zones, for $\geq$2 consecutive days (Rohini et al., 2016; Rajeevan et al., 2023). Cooling Degree Days (CDD24) use base 24°C

consistent with BEE India and ASHRAE Standard 55 tropical comfort standards. Heating Degree Days (HDD18, base 18°C) are physically meaningful only for the Himalayan zones.

Crop-specific seasonal GDD were computed as $\Sigma \max(0, T_t - T_{base})$ over each zone's dominant crop growing season, where T_t = (Tmax + Tmin)/2 and T_{base} is the crop-specific base temperature derived from published Indian researchers, i.e., 5°C for rabi wheat (Mishra et al., 2007; Kumar et al., 2022), 10°C for kharif rice, pearl millet, and sorghum (Kashyapi et al., 2010), 5°C for mustard and rabi pulses (Kumar et al., 2022), 14°C for groundnut (Singh et al., 1994), 15.5°C for cotton (Ban et al., 2015; Kaur et al., 2024), 4.5°C for apple (Qayoom et al., 2022), and 10°C for coconut and plantation crops. An upper temperature cap was applied to Tmax and Tmin before computing T^T (30°C for wheat; 35–40°C for *kharif* crops) to prevent extreme-day GDD inflation, following FAO Irrigation and Drainage Paper 56 upper-cap methodology (Allen et al., 1998). The wheat *rabi* season spans October of year Y to March of year Y+1 and is attributed to harvest year Y+1.

Table 2: Definitions, units, and agronomic significance of selected ETCCDI and India-specific temperature extreme indices computed in this study

Index	Name	Definition (ETCCDI standard)	Unit	Agronomic significance
TXx	Maximum Tmax	Annual maximum value of daily maximum temperature (TX).	°C	Represents extreme heat events causing pollen sterility, forced senescence, and yield loss in crops such as wheat, rice, and maize.
TNx	Maximum Tmin	Annual maximum value of daily minimum temperature (TN).	°C	Indicates extreme warm nights, which increase plant respiration and reduce grain filling efficiency.
TXn	Minimum Tmax	Annual minimum value of daily maximum temperature.	°C	Reflects unusually cold daytime conditions that may suppress photosynthesis and delay crop development.
TNn	Minimum Tmin	Annual minimum value of daily minimum temperature.	°C	Represents extreme cold or frost events, potentially damaging seedlings, reproductive organs, and horticultural crops.
TX90p	Warm Days	Percentage of days when daily maximum temperature exceeds the 90th percentile of the baseline period (1961–1990).	% of days	Indicates increasing frequency of hot days, associated with higher evapotranspiration and irrigation demand.
TN90p	Warm Nights	Percentage of days when daily minimum temperature exceeds the 90th percentile of the baseline period.	% of days	Reflects warmer nights, reducing crop recovery from daytime heat stress and increasing respiration losses.
TX10p	Cold Days	Percentage of days when daily maximum temperature falls below the 10th	% of days	Represents increased frequency of cold daytime conditions, potentially delaying crop growth stages.

		percentile of the baseline period.		
TN10p	Cold Nights	Percentage of days when daily minimum temperature falls below the 10th percentile of the baseline period.	% of days	Indicates cold nights or frost-prone conditions, which may damage crops during flowering or early vegetative stages.
DTR	Diurnal Temperature Range	Mean difference between daily maximum and minimum temperatures (TX − TN).	°C	Influences crop photosynthesis, respiration balance, and grain development.
SU	Summer Days	Annual count of days when TX > 25°C.	days	Represents general heat exposure during the growing season, influencing crop water demand and phenological development.
SU35	Very Hot Days	Annual count of days when TX ≥ 35°C.	days	Indicates severe heat stress causing flower abortion, reduced pollination, and yield reduction in many crops.
TR	Tropical Nights	Annual count of days when TN > 20°C.	days	Reflects persistent warm nights, associated with increased respiration losses and reduced crop productivity.
GDD	Growing Degree Days	Accumulated heat units calculated as Σ[(Tmax + Tmin)/2 − Tb], where Tb is the crop-specific base temperature.	°C·day	Measures thermal time required for crop growth and development, widely used for predicting phenological stages and crop duration.

2.5 Statistical Trend Analysis

Monotonic trends in each climatic index were assessed using the non-parametric Mann–Kendall (MK) test (Mann, 1945; Kendall, 1975). To address the tendency of positive serial autocorrelation in climate time series to inflate the MK test Type I error rate, trend-free pre-whitening (TFPW) was applied to all zone-mean annual series prior to significance testing, following Yue and Wang (2004). Trend magnitudes per decade were quantified using the Sen slope estimator (Sen, 1968). Sub-period analyses were conducted for 1951–1980 and 1981–2025 to assess whether trend magnitudes and statistical significance have intensified in the more recent period. The 75-year record was additionally partitioned into three 25-year temporal blocks i.e. Baseline (1951–1975), Transition (1976–2000), and Contemporary (2001–2025). The inter-block differences were computed to quantify regime shifts. Statistical significance was evaluated at $p < 0.05$ (two-tailed).

3. Results

3.1 Long-term Sen Slope Trends: Full Index Suite

The Sen slope results (Table 3) reveal a thermally heterogeneous yet broadly warming landscape across India's agro-climatic domain. Tropical Nights (TR20; Tmin ≥ 20°C) show the most consistent and agronomically significant positive trends across the mainland zones,

with ten of twelve Tier A/B zones recording statistically significant increases. The highest TR20 Sen slope is observed in ACZ-14 (Western Dry Region; +3.182 days decade^{-1}; $p < 0.05$), followed by ACZ-11 (East Coast Plains; +2.593 days decade^{-1}), ACZ-12 (West Coast Plains and Ghats; +2.500 days decade^{-1}), and ACZ-13 (Gujarat Plains; +1.552 days decade^{-1}). Non-significant TR20 trends are confined to ACZ-10 (Southern Plateau; +0.556 days decade^{-1}) and ACZ-6 (Trans-Gangetic Plain; +1.053 days decade^{-1}), the latter consistent with the documented suppression of daytime heat extremes by intensive irrigation over the Indo-Gangetic Plain, which by increasing near-surface humidity and latent heat flux also moderates the boundary layer thermal environment at night relative to non-irrigated regions, restraining TR20 escalation (Bonfils and Lobell, 2007; Thiery et al., 2020). The significant negative SU35 trends in ACZ-3, ACZ-5, and ACZ-6 are physically consistent with the irrigation-induced suppression of peak Tmax documented by the negative TXx trends in these same zones; expanding groundwater irrigation since the 1960s has increased latent heat flux sufficiently to suppress afternoon maxima below the 35°C threshold more frequently, even as nocturnal temperatures and percentile-based warm-day frequency (TX90p) continue to rise. Over the 75-year study period, the cumulative increase in tropical night frequency in ACZ-14 amounts to approximately 19 additional tropical nights per year, a profound transformation of the nocturnal thermal environment in a desert zone historically distinguished by its large diurnal amplitude, with severe consequences for pearl millet and livestock thermoregulation.

Table 3. Sen slope estimates (per decade) for selected temperature extreme indices across 14 Indian agro-climatic zones. Asterisk (*) denotes statistical significance at $p < 0.05$ (Mann–Kendall test with trend-free pre-whitening; Yue and Wang, 2004). Units: °C decade^{-1} for TXx, TNn, DTR; % decade^{-1} for TX90p; days decade^{-1} for TR20, SU25. Dash (—) = not computed (Tier C). Zones ordered by ACZ number.

ACZ No.	TXx	TNn	TX90p	TN90p	DTR	TR20	SU25^{+}	SU35
1	-0.066	0.235*	1.772*	2.100*	-0.050*	—	—	—
2	0.331*	0.147*	4.721* ‡	2.740*	0.047*	—	—	—
3	−0.111	0.104*	1.300*	3.876*	−0.111*	1.714*	−0.667*	-1.071*
4	−0.152*	−0.027	0.863*	1.159*	−0.059*	0.667*	0.196	0.172
5	−0.081*	0.045	0.257	1.703*	−0.100*	0.769*	0.476	-1.177*
6	−0.034	0.138*	0.068	1.775*	−0.105*	1.053	0.732	-1.207*
7	−0.181*	−0.003	0.981*	1.724*	−0.042*	1.183*	−1.000*	-0.191
8	0.097	0.098*	0.548*	1.536*	−0.068*	1.250*	0.000	1.250*
9	0.136*	0.007	1.111*	0.953*	−0.001	1.064*	−0.400*	0.000*
10	0.161*	−0.004	2.962*	1.068*	0.097*	0.556	0.000*	1.053*
11	0.093*	0.090*	2.940*	1.176*	0.076*	2.593*	0.000*	3.143*
12	0.095*	0.048*	2.917*	2.554*	0.044*	2.500*	0.000*	1.875*
13	0.137*	0.173*	1.154*	1.565*	−0.020	1.552*	−0.312	2.326*
14	0.254*	0.250*	1.222*	4.384*	−0.249*	3.182*	0.541	2.000*

+SU25 (Summer Days; Tmax > 25°C) is retained for global comparability only; SU35 (Hot Days; Tmax ≥ 35°C) is the primary India-relevant warm-day threshold in this study, consistent with WMO Climpact v2 and published agronomic heat-stress thresholds.

‡ ACZ-2 (Tier C, Eastern Himalayan Region) TX90p trend should be interpreted with caution: the sparse observational network in high-elevation terrain during the 1969–1990 base period may affect percentile estimation. Results are presented as indicative.

Annual maximum of daily maximum temperature (TXx) trends are more spatially heterogeneous than TR20. The strongest significant positive TXx trends occur in ACZ-14 (Western Dry Region; +0.254°C decade^{-1}; $p < 0.05$), ACZ-10 (Southern Plateau; +0.161°C decade^{-1}), and ACZ-13 (Gujarat Plains; +0.137°C decade^{-1}). Across the Gangetic belt, significant negative TXx trends are recorded in ACZ-4 (Middle Gangetic Plain; −0.152°C decade^{-1}; $p < 0.05$) and ACZ-5 (Upper Gangetic Plain; −0.081°C decade^{-1}), while ACZ-3 (Lower Gangetic Plain) shows a non-significant decrease (−0.111°C decade^{-1}). These opposing TXx signals in the Gangetic zones reflect the competing influences of irrigation-induced evaporative cooling which has expanded enormously across the Gangetic basin since the 1970s and increased monsoon cloudiness associated with strengthened moisture flux from the Bay of Bengal, both of which suppress peak daytime temperatures while leaving nocturnal minima relatively unaffected (Bonfils and Lobell, 2007; Kothawale et al., 2010). The co-occurrence of declining or stable TXx with rising TR20 in ACZ-3, ACZ-4, and ACZ-5 constitutes unambiguous evidence of asymmetric nocturnal warming in the eastern Gangetic domain.

The annual minimum of daily minimum temperature (TNn) shows significant warming in ACZ-14 (Western Dry Region; +0.250°C decade^{-1}; $p < 0.05$), ACZ-13 (Gujarat Plains; +0.173°C decade^{-1}), ACZ-6 (Trans-Gangetic Plain; +0.138°C decade^{-1}), ACZ-11 (East Coast Plains; +0.090°C decade^{-1}), and ACZ-3 (Lower Gangetic Plain; +0.104°C decade^{-1}). The warming of TNn in ACZ-14, historically the zone with some of the lowest annual minimum temperatures across the Indian plains, has significant agricultural implications: pearl millet and cluster bean benefit from warm-night pre-germination soil temperatures, but sustained elevation of nocturnal minima during the reproductive phase also accelerates dark respiration and reduces net carbon gain per unit of accumulated heat. In ACZ-6, which encompasses Punjab, Haryana, and the Delhi region, India's highest-intensity wheat-producing belt, the continued significant TNn warming (+0.138°C decade^{-1}) alongside DTR narrowing signals that the cold-season thermal environment is being compressed from both ends simultaneously, with implications for vernalisation efficiency and overwintering pathogen survival.

Warm-day frequency (TX90p) shows significant positive trends across nine Tier A/B zones, with the highest Sen slopes in ACZ-10 (Southern Plateau; +2.962% decade^{-1}), ACZ-11 (East Coast Plains; +2.940% decade^{-1}), and ACZ-12 (West Coast/Ghats; +2.917% decade^{-1}). Gujarat Plains (ACZ-13; +1.154% decade^{-1}), ACZ-14 (Western Dry Region; +1.222% decade^{-1}), and ACZ-9 (Western Plateau; +1.111% decade^{-1}) also record large significant positive trends (Figure 2). ACZ-3 (Lower Gangetic Plain; +1.300% decade^{-1}) and ACZ-4 (Middle Gangetic Plain; +0.863% decade^{-1}) show significant TX90p increases, despite their declining or neutral TXx trends, reflecting the fact that TX90p is referenced against the fixed 1961–1990 baseline percentile and thus registers increasing warm-day exceedance even when the absolute peak temperature is not rising. The co-occurrence of large TX90p increases alongside strong TR20 trends in ACZ-11 and ACZ-12 identifies both coastal zones as experiencing comprehensive thermal intensification across the full diurnal cycle, a pattern physically consistent with the positive sea-surface temperature trends documented across the Bay of Bengal and Arabian Sea in recent decades (Rohini et al., 2019). The exceptionally high TX90p Sen slope in ACZ-2 (+4.721% decade^{-1}) warrants cautious interpretation given the sparse Himalayan observational network in the 1969–1990 base period, and is classified as indicative within the Tier C framework.

Figure 2: TR20 annual zone-mean time series with trend lines shown for visual reference for all Tier A and Tier B ACZs, 1951–2025. Note the steepest positive trend in ACZ-14 (Western Dry Region) followed by ACZ-11 (East Coast Plains) and ACZ-12 (West Coast/Ghats). Annotated slopes in days per decade. Data source: IMD 1°×1° gridded daily

temperature dataset; grid centroids assigned to ACZs using the region code field of the ICAR/Planning Commission shapefile

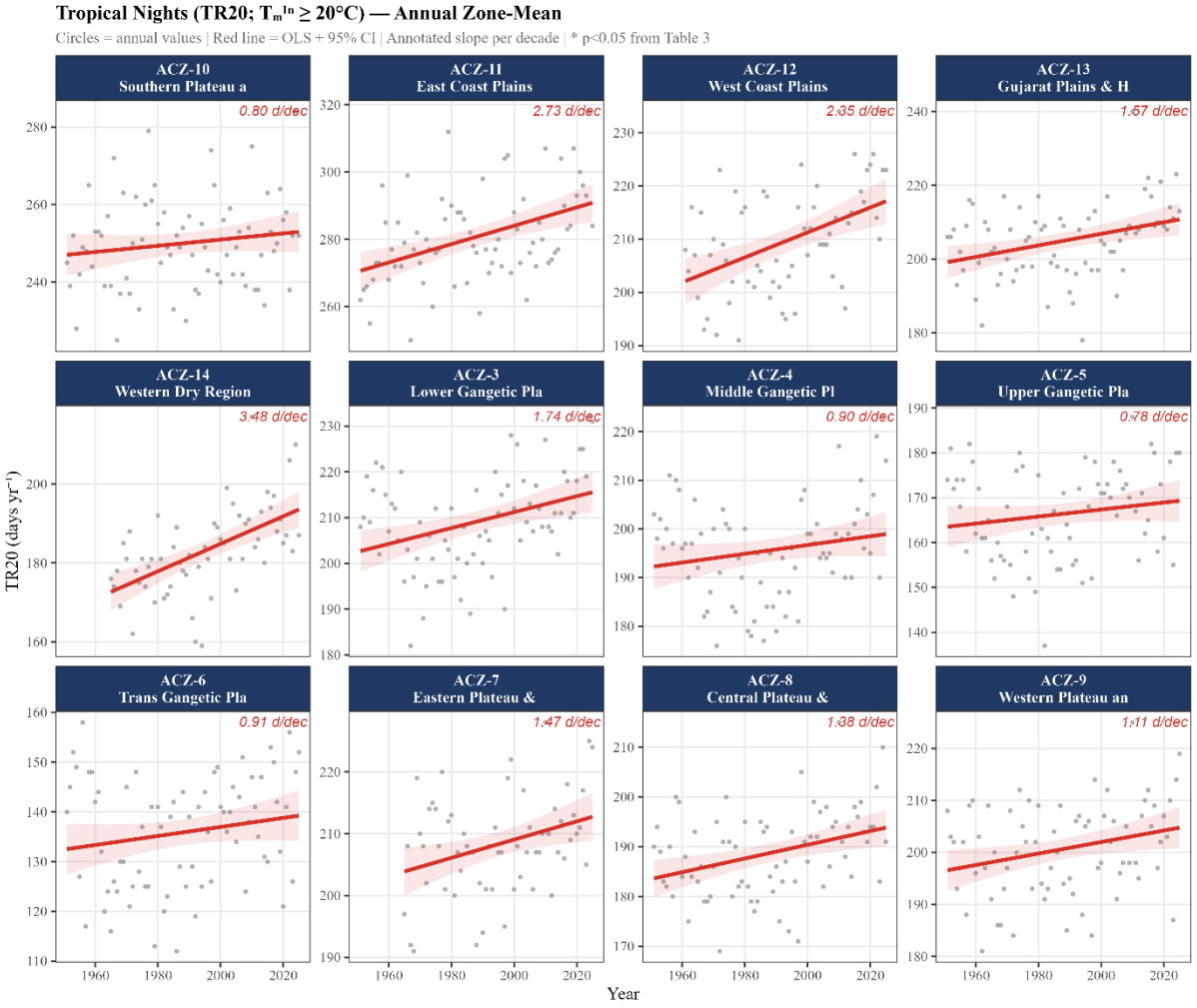

3.2 Diurnal Temperature Range: Asymmetric Warming Diagnosis

The DTR index provides the most direct diagnostic of daytime *versus* night-time warming asymmetry. Significantly negative DTR trends, indicating that Tmin is rising faster than Tmax, are observed in seven Tier A/B zones (Figure 3): ACZ-14 (Western Dry Region; −0.249°C decade^{-1}; $p < 0.05$), ACZ-3 (Lower Gangetic; −0.111°C decade^{-1}), ACZ-6 (Trans-Gangetic Plain; −0.105°C decade^{-1}), ACZ-5 (Upper Gangetic; −0.100°C decade^{-1}), ACZ-8 (Central Plateau; −0.068°C decade^{-1}), ACZ-4 (Middle Gangetic; −0.059°C decade^{-1}), and ACZ-7 (Eastern Plateau; −0.042°C decade^{-1}. The pronounced narrowing in ACZ-14 reflects greenhouse-forced nocturnal warming overriding the historically large desert diurnal amplitude, while the persistent narrowing in ACZ-6 is consistent with the documented expansion of groundwater-based irrigation across Punjab and Haryana since the Green Revolution (1960s–2000s), which has dramatically increased near-surface atmospheric humidity, cloud fraction, and nocturnal moisture emission from irrigated fields, collectively suppressing radiative cooling at night while partially moderating peak afternoon temperatures through evaporative cooling (Kothawale et al., 2010). Over 75 years, the cumulative DTR reduction in ACZ-6 amounts to approximately 0.79°C, a compression of the daily thermal cycle with direct relevance to crop quality parameters such as wheat kernel hardness and sugar accumulation in sugarcane.

Figure 3: Spatial distribution of DTR Sen slope (°C decade⁻¹) by ACZ. Blue bars/shading = Tmin rising faster than* Tmax *(negative DTR; greenhouse forcing fingerprint). Red =* Tmax *rising faster. * p < 0.05

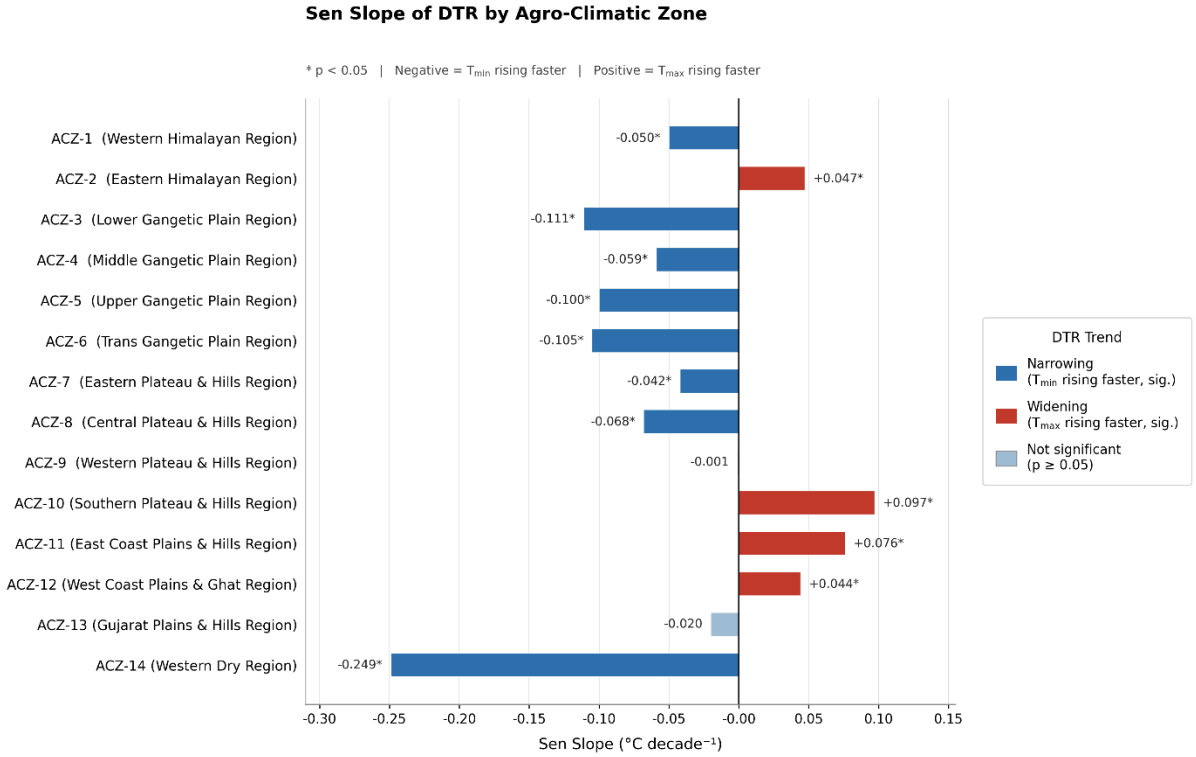

Significantly positive DTR trends, indicating daytime warming outpacing nocturnal warming, are recorded in ACZ-10 (Southern Plateau; +0.097°C decade⁻¹), ACZ-11 (East Coast Plains; +0.076°C decade⁻¹), and ACZ-12 (West Coast/Ghats; +0.044°C decade⁻¹). The positive DTR in these southern and coastal zones co-occurs with the highest TX90p trends in the domain, indicating that daytime warming is genuinely outpacing nocturnal warming in these regions. The moderate positive DTR in ACZ-12 (+0.044°C decade⁻¹) alongside a still-substantial TR20 trend (+2.500 days decade⁻¹) and significant TXx increase (+0.095°C decade⁻¹) confirms that both ends of the daily temperature cycle are warming in the West Coast zone, with daytime Tmax rising slightly faster than Tmin. This pattern is physically consistent with reduced pre-monsoon cloud cover driven by changing Arabian Sea moisture flux (Rohini et al., 2019).

3.3 Crop-Specific Growing Degree Day Trends

Seasonal GDD analysis reveals crop-specific thermal time accumulation trends with direct agronomic significance (Figure 4). *Rabi* wheat GDD (base 5°C, October–March, attributed to harvest year) increased significantly in ACZ-6 (Trans-Gangetic Plain; +11.130 GDD decade⁻¹; $p < 0.05$) and ACZ-13 (Gujarat Plains; +21.625 GDD decade⁻¹) zones that support India's most economically important wheat and wheat-cotton systems, respectively. In ACZ-5 (Upper Gangetic Plain), the wheat GDD trend (+3.255 GDD decade⁻¹) is positive but does not reach statistical significance at $p < 0.05$, suggesting that the irrigation-induced suppression of Tmax partially offsets rising Tmin in the seasonal thermal accumulation. Accelerating GDD accumulation in ACZ-6 shortens the effective grain-filling period by advancing phenological transitions from anthesis to physiological maturity, reducing the time available for carbon translocation into the grain. The combination of rising *rabi* GDD with significant DTR narrowing (−0.100°C decade⁻¹) in ACZ-5 compounds thermal stress from both ends: not only is the growing season thermally accelerated, but the nocturnal recovery window that partially

offsets daytime heat stress is being progressively shortened (Misra et al., 2019a; Pal et al., 2008). These findings are directly relevant to the calibration of CERES-wheat model simulations for Indian conditions, where GDD is the primary driver of phenological progression.

For the West Coast zone (ACZ-12), the dominant plantation crops (coconut, spices, rubber, and coffee) operate under year-round high temperatures and have narrow thermal optima. The significant TR20 trend (+2.500 days decade^{-1}) alongside the largest GDD_C1 increase in the domain (+33.725 GDD decade^{-1}; $p < 0.05$) means that the thermal time environment experienced by these perennial crops has shifted measurably away from baseline conditions, with cumulative effects on flowering phenology, fruit development, and long-term productivity compounding over the multi-decade lifespans of individual plants. Annual GDD accumulation for coconut (base 10°C, annual season) in ACZ-12 has correspondingly increased by approximately 163 GDD (Contemporary vs Baseline blocks), reducing the number of days near the lower end of the thermal optimum and potentially advancing inflorescence emergence timing (Kingra and Misra, 2021).

Figure 4: Seasonal GDD trend plots: (a) rabi wheat (base 5°C, Oct–Mar) in ACZ-5 and ACZ-6; (b) kharif cotton (base 15.5°C, Apr–Oct) in ACZ-8, ACZ-9, and ACZ-13. Trend lines shown for visual reference with per-decade annotations. Source: IMD gridded Tmax/Tmin, pipeline with corrected ACZ region code assignment.

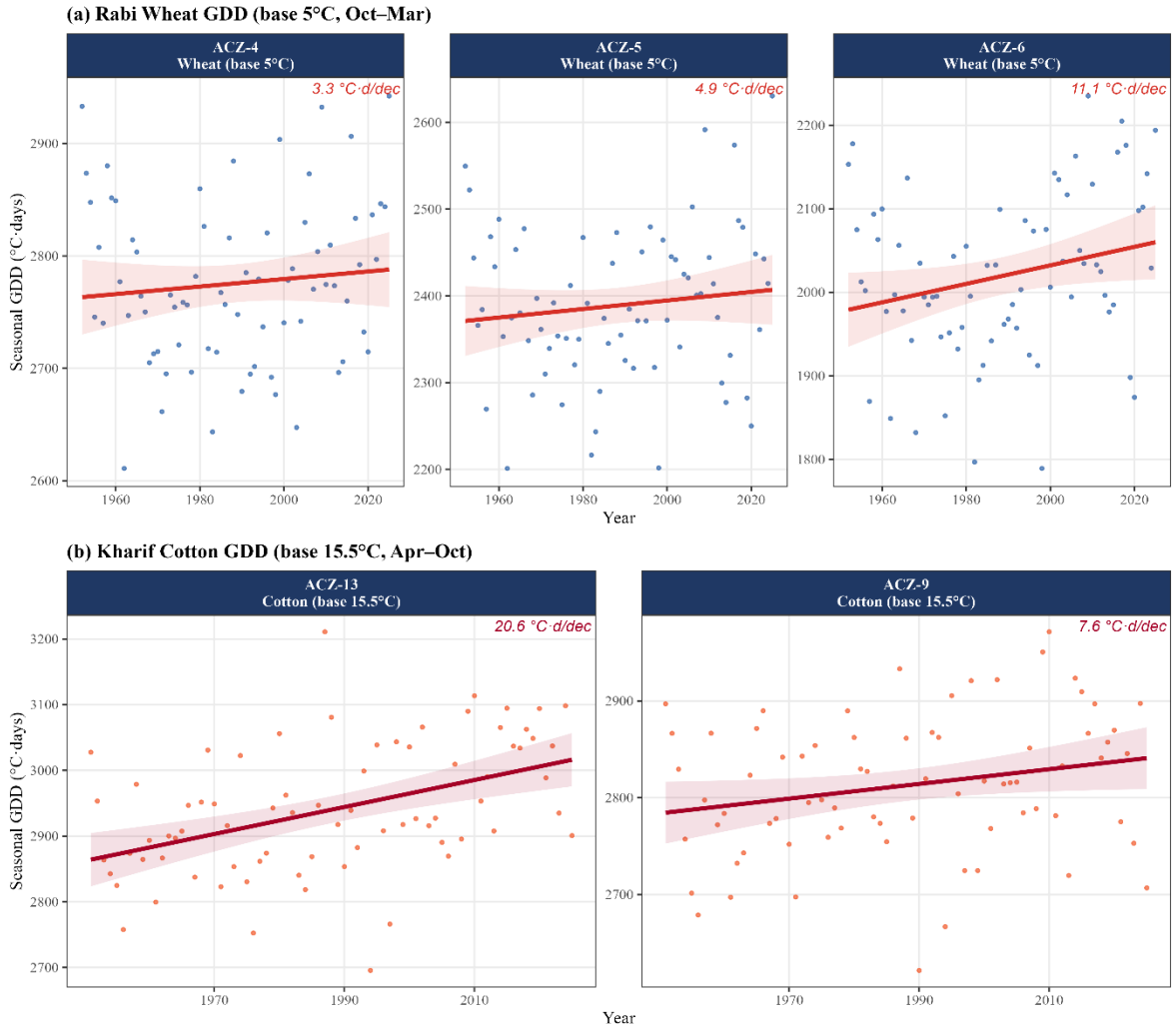

3.4 Temporal Block Analysis: Identification of a Warming Regime Shift

Partitioning the record into 25-year temporal blocks (Figure 5) reveals a clear and accelerating thermal progression. During the Baseline period (1951–1975), TR20 frequencies were close to their long-term climatological means in most zones, with ACZ-11 (East Coast Plains) averaging approximately 273 tropical nights annually and ACZ-12 (West Coast/Ghats) averaging approximately 205 tropical nights, values consistent with their tropical-humid climatic character. ACZ-14 (Western Dry Region) averaged approximately 177 tropical nights during the Baseline, reflecting substantial warm-season nocturnal heat retention even in the Thar Desert. The Transition block (1976–2000) shows the onset of significant TR20 increases in the western, coastal, and arid zones, broadly consistent with the documented post-1980 acceleration of Indian Ocean warming and its influence on land temperatures (Rohini et al., 2019). In the Contemporary block (2001–2025), every Tier A/B zone records TR20 zone-mean values exceeding the respective Baseline mean, with the largest absolute increases in ACZ-14 (+13.92 days year^{-1}), ACZ-11 (+12.96 days year^{-1}), and ACZ-13 (+8.44 days year^{-1}). The majority of annual TR20 records across all zones have been set in the period after 2010, consistent with WMO (2024) confirmation that 2015–2024 constitutes the globally warmest decade on record.

Figure 5: Decadal-mean TR20 bar plots for all Tier A and Tier B ACZs (1951–2025). Colour progression from cool blue (1951–60) to dark red (2021–25). Horizontal dashed lines indicate 25-year block means. The monotonic escalation from Baseline through Transition to Contemporary is most pronounced in ACZ-14, ACZ-11, and ACZ-13.

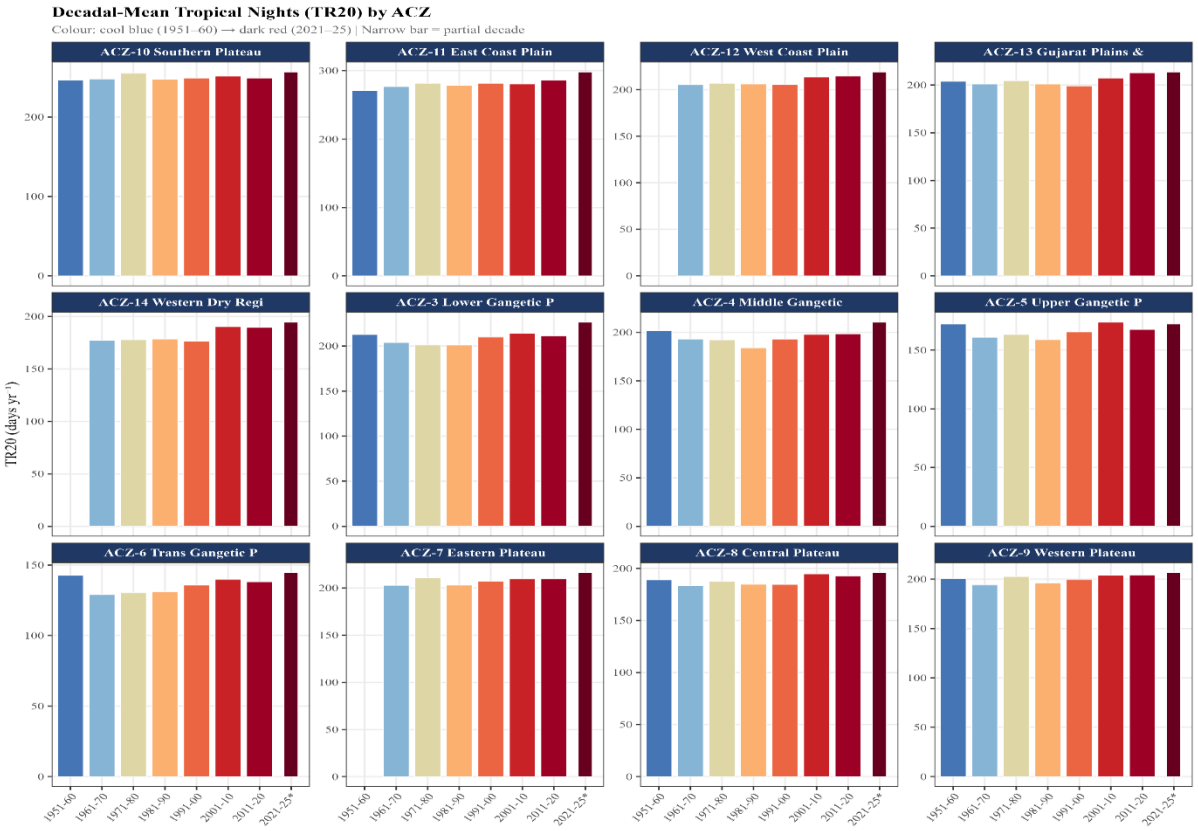

4. Discussion

4.1 Western Dry Region (ACZ-14): Unexpected Thermal Leader Across Multiple Metrics

The analysis yields a finding that is climatologically counterintuitive: ACZ-14 (Western Dry Region, encompassing the Thar Desert of western Rajasthan and parts of Gujarat) records not only the highest TR20 trend in the 14-zone domain (+3.182 days decade^{-1}; $p < 0.05$) but simultaneously the strongest DTR narrowing (−0.249°C decade^{-1}) and the highest TXx

warming (+0.254°C decade⁻¹). This triple thermal intensification, i.e., more tropical nights, more hot days, and a rapidly narrowing diurnal range, identifies ACZ-14 as the compound thermal hotspot of Indian agriculture in the 1951–2025 record. In arid systems, night time temperatures are generally suppressed by intense long-wave emission from cloudless, dry skies; the observed trend of +3.182 days decade⁻¹, resulting approximately 19 additional tropical nights per year over the study period, signals that greenhouse gas-forced nocturnal warming and increasing tropospheric water vapour are now overriding the historically large diurnal amplitude of the desert climate. Fischer and Knutti (2015) demonstrated that anthropogenic forcing disproportionately raises extreme temperatures in low-moisture land surfaces; the ACZ-14 results provide direct empirical support for this mechanism in an agronomically active arid landscape. The agronomic implications are severe across multiple timescales. Pearl millet, the dominant *kharif* staple of the Thar Desert fringe, is among the most heat-tolerant cereal crops yet exhibits spikelet sterility when panicle temperatures exceed 42°C during anthesis; the combination of rising TXx (+0.254°C decade⁻¹) and declining nocturnal recovery (DTR −0.249°C decade⁻¹) progressively extends the duration of acute heat exposure during critical reproductive stages. For the zone's substantial livestock population, the erosion of cool desert nights reduces the nocturnal window for metabolic heat dissipation in cattle, sheep, and camel herds, with implications for feed conversion efficiency and reproductive performance that parallel findings from other arid pastoral systems (Das et al., 2016).

4.2 Coastal Thermal Intensification: East Coast Plains (ACZ-11) and West Coast Plains and Ghats (ACZ-12)

The East Coast Plains and Hills (ACZ-11) recorded the second-highest TR20 trend (+2.593 days decade⁻¹; $p < 0.05$), along with the second-highest TX90p increase (+2.940% decade⁻¹), significant TXx warming (+0.093°C decade⁻¹), and TNn warming (+0.090°C decade⁻¹). This zone, covering coastal Andhra Pradesh, Tamil Nadu, and Odisha, is experiencing thermal intensification across the diurnal cycle. Co-occurring TR20 and TX90p trends indicate synchronous night- and daytime extremes, driven by Bay of Bengal warming and limited inland penetration of maritime moisture sustaining high nocturnal humidity. For kharif rice, rising TR20 during panicle initiation and heading elevates spikelet sterility risk. Mohan and Kandya (2015) noted urban heat island amplification of nocturnal extremes; the gridded signals here likely include both background climate change and urban effects requiring station-level separation.

The West Coast Plains and Ghats (ACZ-12) records the third-highest TR20 (+2.500 days decade⁻¹) and TX90p (+2.917% decade⁻¹). A significant SU35 increase (+1.875 days decade⁻¹) shows expansion of Tmax ≥ 35°C days, compressing thermal comfort for crops and workers. Rising SU35, TR20, and TX90p without decline in TXx confirms warming across the full daytime temperature distribution.

4.3 Gangetic Plains: Irrigation-Modulated Asymmetric Warming

The Gangetic zones (ACZ-3 to ACZ-6) present a contrasting and mechanistically informative pattern: declining or stable TXx trends alongside significant TR20 increases, combined with pervasive DTR narrowing across all four zones (ACZ-3: −0.111°C decade⁻¹; ACZ-4: −0.059°C decade⁻¹; ACZ-5: −0.100°C decade⁻¹; ACZ-6: −0.105°C decade⁻¹; all $p < 0.05$). The significant negative TXx trends in ACZ-4 (−0.152°C decade⁻¹) and ACZ-5 (−0.081°C decade⁻¹), at first counter-intuitive in a warming world, are physically consistent with several well-documented processes: the massive expansion of irrigation water application since the 1960s has substantially increased latent heat flux at the surface, diverting a larger fraction of solar energy into evaporation rather than sensible heating and thereby suppressing peak daytime temperatures (Kothawale et al., 2010). Simultaneously, increased aerosol loading from industrial and agricultural burning sources reduces surface solar radiation receipt, further

dampening Tmax while having minimal effect on the long-wave-dominated night-time energy balance. The result is asymmetric warming, uniquely characteristic of intensively irrigated, aerosol-loaded agricultural systems, a pattern with important implications for interpreting climate model projections that may under-represent the irrigation-cooling effect. Notably, TR20 in ACZ-6 (Trans-Gangetic Plain) is non-significant (+1.053 days decade^{-1}, $p > 0.05$), reflecting the complex interplay between greenhouse warming and irrigation-induced surface cooling in this most intensively managed zone.

For wheat cultivation in ACZ-6 (Punjab/Haryana/western UP, the Trans-Gangetic Plain), the combination of significantly rising rabi GDD (+11.130 GDD decade^{-1}; $p < 0.05$), significantly warming TNn (+0.138°C decade^{-1}), and DTR narrowing (−0.105°C decade^{-1}) signals a progressive narrowing of the thermal window optimal for grain filling. This contrast arises because GDD integrates cumulative daytime and nocturnal temperatures across the full rabi season, whereas TR20 reflects a threshold rarely exceeded during the cool-season months in this zone. The negative, non-significant TXx trend (−0.034°C decade^{-1}) means that irrigation-induced evaporative cooling is still successfully moderating peak daytime heat stress during the critical anthesis-to-maturity window but this buffering is not matched at night. The warming TNn trend implies that the coldest nights of the rabi season are becoming systematically warmer, reducing cold-season vernalisation efficiency for winter wheat varieties that require prolonged chilling for adequate tiller development. Misra et al. (2019b) documented the meteorological drivers of plant disease development; the warming winter minimum temperature regime simultaneously expands the thermal suitability window for wheat yellow rust and other overwintering fungal pathogens, adding a phytopathological dimension to the already-documented thermal stress trajectory. The significant rabi GDD increase in ACZ-13 (+21.625 GDD decade^{-1}; $p < 0.05$) alongside substantial TR20 increase (+1.552 days decade^{-1}) and rising TXx (+0.137°C decade^{-1}) identifies Gujarat's dual wheat-cotton system as facing compound thermal pressure from multiple directions simultaneously.

4.4 Gujarat Plains (ACZ-13) and Western Dry Region (ACZ-14): Compound Thermal Hotspots

As detailed in Section 4.1, ACZ-14 records the most comprehensive multi-index thermal compression of any zone, with the highest TR20 (+3.182 days decade^{-1}), strongest DTR contraction (−0.249°C decade^{-1}), and highest TXx warming (+0.254°C decade^{-1}) in the domain and a significant TNn increase (+0.250°C decade^{-1}). Gujarat Plains (ACZ-13) records the largest rabi wheat GDD increase in the domain (+21.625 GDD decade^{-1}; $p < 0.05$), confirming that accumulated thermal time for winter crops is increasing rapidly even in zones where monsoon-season heat stress may not be the dominant agronomic constraint.

4.5 Contextualisation within Published Literature

The overall pattern documented in this study, widespread TR20 increase, pervasive DTR narrowing across eight Tier A/B zones, TX90p intensification in coastal and plateau regions, and warming acceleration in the post-2000 period, is broadly consistent with global findings from HadEX2 (Donat et al., 2013) and IPCC AR6 (IPCC, 2021). The global analysis of Alexander et al. (2006) identified South Asia as a region with a significant increase in warm nights in the global ETCCDI dataset; the present study extends this finding through 2025 at ACZ-level spatial resolution and reveals that the highest TR20 trend occurs in the Western Dry Region (ACZ-14). The coastal zones (ACZ-11, ACZ-12) record the largest TX90p increases, consistent with the maritime thermal amplification mechanism. The asymmetric nocturnal warming pattern (TN90p > TX90p) holds across nine zones but is reversed in the coastal and southern plateau zones (ACZ-9, ACZ-10, ACZ-11, ACZ-12), where TX90p substantially exceeds TN90p, consistent with reduced maritime cloud cover and land-surface sensible heat amplification in these regions. The DTR narrowing detected in 8 Tier A/B zones substantially

expands upon the 5 reported in earlier zone-aggregated Indian analyses; the additional detection in ACZ-7 (Eastern Plateau; −0.042°C decade^{-1}) and ACZ-8 (Central Plateau; −0.068°C decade^{-1}) extends the irrigation- and aerosol-amplified cooling signal deeper into the Deccan interior than previously documented, consistent with the expansion of tank irrigation and drip systems across these zones since the 1990s. DTR narrowing in the Gangetic zones is consistent with Kothawale et al. (2010), who documented differential warming of minimum versus maximum temperatures across the Indian long-term record, while findings for Gujarat align with Pandey et al. (2017, 2019), who documented climate change impacts on Gujarat and Indian crop production through ENSO-linked thermal anomalies. The accelerating warming in the post-2000 period is consistent with WMO (2024) confirmation that 2015–2024 constitutes the globally warmest decade on record, and with Jain et al. (2013) who documented systematic temperature trend increases in northeast India. These findings extend CERES-wheat calibration frameworks for Indian conditions (Pal et al., 2008; Misra et al., 2019a) by confirming that the thermal time environment is itself a non-stationary, zone-dependent system.

5. Limitations and Uncertainties

Several inherent limitations of the gridded temperature approach warrant explicit acknowledgement. The representativeness of the IMD 1°×1° dataset is highest over continental interior plains and degrades considerably in regions of complex terrain. In ACZ-1 (Western Himalayan) and ACZ-2 (Eastern Himalayan), individual grid cells span elevation ranges of 3,000–5,000 m, meaning interpolated values represent network-density-weighted spatial averages with no correspondence to any actual location within the cell. The orographic temperature lapse rate of approximately 6°C km^{-1} introduces systematic representativeness errors irrecoverable from the gridded product alone, motivating both the Tier C analytical framework and the restriction of Himalayan results to a subset of robust indices. In ACZ-12 (West Coast Plains and Ghats), steep orographic gradients across the coastal–highland transition within a single grid cell introduce additional uncertainty in absolute index values, though trend directions remain likely robust given their magnitudes. As the study objective is to assess long-term regional trends across ACZs rather than local microclimatic variability, ACZ-level spatial aggregation mitigates much of the grid-scale heterogeneity in trend estimates.

Network non-stationarity over the 75-year record represents a further source of potential confounding. The IMD surface observatory network expanded substantially through the 1960s and 1980s, and the transition to automatic weather stations from the mid-1990s altered both sampling density and instrumentation characteristics. Although IMD quality-control procedures are designed to minimise such effects, independent homogenisation across all grid cells has not been comprehensively verified. Uncertainty is greatest in the early record (1951–1965) and in data-sparse regions, which motivated the Tier B truncated start dates; pre-1965 trend estimates in ACZ-7, ACZ-12, and ACZ-14 accordingly carry greater uncertainty than post-1965 counterparts.

Urbanisation is a potentially important confounding factor in several zones. ACZ-6 (Trans-Gangetic Plain) encompasses Delhi, Chandigarh, Ludhiana, and Amritsar, where urban heat island effects can systematically elevate minimum temperatures, potentially amplifying the TR20 and DTR-narrowing trends beyond what rural-only observations would capture (Dash and Mamgain, 2011). ACZ-13 (Gujarat) and ACZ-3 (Lower Gangetic/West Bengal) similarly contain major urban agglomerations that may contribute to the nocturnal warming signal. Disentangling urban from background climate signals requires station-level homogenisation beyond the scope of this gridded-data study; future work should explicitly quantify urban heat island contributions through rural–urban station pair analysis within each ACZ.

Finally, the use of a fixed 1961–1990 WMO base period for percentile computation means that TX90p, TN90p, TX10p, and TN10p measure the changing probability of historically extreme events rather than departures from a contemporaneous climatological normal. This is methodologically appropriate for long-term trend detection but should be clearly communicated when results are applied to current-season agricultural planning or risk assessment. The 1°×1° resolution also precludes detection of sub-zone heterogeneity relevant to district-level management; emerging higher-resolution IMD products (e.g., 0.5°×0.5° grids) could improve spatial specificity in future analyses, though their shorter temporal coverage currently constrains their utility for multi-decadal trend assessment.

6. Conclusions

This study provides a spatiotemporally resolved characterisation of 22 temperature extreme indices across India's 14 mainland Agro-Climatic Zones (ACZs) spanning 1951–2025, with spatial assignment verified against ICAR zone codes, names, and physiographic descriptors. Five principal conclusions emerge.

The Western Dry Region (ACZ-14) exhibits the domain's steepest Tropical Nights trend (+3.182 days decade^{-1}; $p < 0.05$), an outcome that challenges the conventional expectation of large diurnal amplitude in Thar Desert climatology. Greenhouse gas-forced nocturnal warming, reinforced by rising tropospheric water vapour, is evidently overriding this historical diurnal buffering. ACZ-14 concurrently shows the strongest DTR contraction (−0.249°C decade^{-1}) and highest TXx warming (+0.254°C decade^{-1})—a triple thermal compression carrying serious consequences for pearl millet cultivation and pastoral livestock systems across western Rajasthan. The East Coast Plains (ACZ-11; +2.593 days decade^{-1}) and West Coast Plains and Ghats (ACZ-12; +2.500 days decade^{-1}) rank second and third in TR20 trends and lead coastal zones in TX90p increase, reinforcing the necessity of zone-specific rather than nationally aggregated analysis.

DTR narrowing—the clearest fingerprint of asymmetric nocturnal warming—is now statistically detectable in eight Tier A/B zones. Beyond ACZ-14, significant contraction extends continuously through the Gangetic belt (ACZ-3 to ACZ-6) into the Central and Eastern Plateau. Paradoxically, ACZ-4 (Middle Gangetic; −0.152°C decade^{-1}) and ACZ-5 (Upper Gangetic; −0.081°C decade^{-1}) register negative TXx trends alongside rising TR20, a spatially coherent pattern consistent with irrigation-amplified asymmetric warming that diverges markedly from global mean temperature projections.

Gujarat Plains (ACZ-13) record the largest domain-wide GDD increases for both rabi wheat (+21.625 GDD decade^{-1}; $p < 0.05$) and kharif crops (+14.769 GDD decade^{-1}), accompanied by significant TXx warming (+0.137°C decade^{-1}), TR20 rise (+1.552 days decade^{-1}), and SU35 expansion (+2.326 days decade^{-1}). This convergence of daytime, nocturnal, and accumulated thermal extremes designates ACZ-13 as a compound thermal hotspot within India's economically critical cotton–groundnut–dairy corridor.

Significant rabi wheat GDD increases in ACZ-6 (Trans-Gangetic Plain; +11.130 GDD decade^{-1}) and ACZ-13 are compressing grain-filling durations and advancing anthesis into higher-temperature periods. Simultaneous DTR narrowing across the entire Gangetic belt curtails nocturnal crop recovery, collectively signalling a multi-dimensional deterioration of the thermal environment for India's most strategically vital cereal system. Systematic revision of agronomic calendars, variety deployment strategies, and irrigation scheduling across this belt is warranted. The Contemporary block (2001–2025) represents the warmest 25-year epoch across all indices and zones. Future research should prioritise urban–rural signal separation in nocturnal trend attribution, integration with 0.25° IMD gridded data for sub-zone refinement, compound hot-dry extreme quantification, and CMIP6 projection contextualisation to support evidence-based adaptation planning.

CRediT Author Contribution Statement

Ashutosh Kumar Misra: Conceptualization, Data curation, Methodology, Investigation, Visualization, Validation, Writing - original draft, Writing - review & editing. **Sudhir Kumar Mishra:** Writing - review & editing, Software, Methodology, Investigation, Formal analysis. **Santosha Rathod:** Data curation, Investigation, Writing - review & editing. **Kripan Ghosh:** Supervision, Project administration, Writing - review & editing. **Asha Latwal:** Writing - review & editing, Formal analysis, Software, Methodology. **M R Deo:** Data curation, Investigation. **K G Kanade:** Data curation, Investigation.

Declaration of Competing Interests

The authors declare that they have no known competing financial interests or personal relationships that could have appeared to influence the work reported in this paper.

Data Availability

The IMD 1°×1° gridded daily temperature dataset is available from the India Meteorological Department (https://imdpune.gov.in). The ACZ shapefile is available from the Open Government Data Platform India (https://www.data.gov.in/resource/boundaries-agro-climatic-regions).

Acknowledgements

The authors gratefully acknowledge the India Meteorological Department (IMD), Pune, for providing the gridded daily temperature dataset used in this study.

Funding

This research did not receive any specific grant from funding agencies in the public, commercial, or not-for-profit sectors.

Declaration of generative AI use

The authors used Claude (Anthropic) and ChatGPT (OpenAI) for language editing, structural revision, and assistance with journal formatting. These tools were not used for data collection, statistical analysis, interpretation of results, or generation of scientific conclusions. All scientific content, including the analysis, results, and conclusions, is solely the responsibility of the human authors.

References

Alexander LV, Zhang X, Peterson TC, Caesar J, Gleason B, Klein Tank AMG, Haylock M, Collins D, Trewin B, Rahimzadeh F, Tagipour A, Rupa Kumar K, Revadekar J, Griffiths G, Vincent L, Stephenson DB, Burn J, Aguilar E, Brunet M, Taylor M, New M, Zhai P, Rusticucci M, Vazquez-Aguirre JL. 2006. Global observed changes in daily climate extremes of temperature and precipitation. Journal of Geophysical Research: Atmospheres, 111(D5): D05109. https://doi.org/10.1029/2005JD006290

Allen RG, Pereira LS, Raes D, Smith M. 1998. Crop Evapotranspiration: Guidelines for Computing Crop Water Requirements. FAO Irrigation and Drainage Paper 56. Food and Agriculture Organization: Rome. https://www.fao.org/4/x0490e/x0490e00.htm

Ban, Y. G., Nawalkar, D. P., Mote, B. M., Kumar, V. & Narwade, A. V. 2015 Crop phenology, thermal requirement, yield and fiber properties of cotton (Gossypium hirsutum) genotypes as influenced by different environments. International Journal of Plant Physiology 20, 137–144. https://doi.org/10.1007/S40502-015-0153-8

Bonfils C, Lobell D. 2007. Empirical evidence for a recent slowdown in irrigation-induced cooling. Proceedings of the National Academy of Sciences, 104(34): 13582–13587. https://doi.org/10.1073/pnas.0700144104

Bronaugh D. 2020. climdex.pcic: PCIC Implementation of Climdex Routines. R package version 1.1-11. https://CRAN.R-project.org/package=climdex.pcic

Das R, Sailo L, Verma N, Bharti P, Saikia J, Imtiwati, Kumar R. 2016. Impact of heat stress on health and performance of dairy animals: a review. Veterinary World, 9(3): 260–268. https://doi.org/10.14202/vetworld.2016.260-268

Dash SK, Mamgain A. 2011. Changes in the frequency of different categories of temperature extremes in India. Journal of Applied Meteorology and Climatology, 50(9): 1842–1858. https://doi.org/10.1175/2011JAMC2687.1

Donat MG, Alexander LV, Yang H, Durre I, Vose R, Dunn RJH, Willett KM, Aguilar E, Brunet M, Caesar J, Hewitson B, Jack C, Klein Tank AMG, Kruger AC, Marengo J, Peterson TC, Renom M, Oria Rojas C, Rusticucci M, Salinger J, Elrayah AS, Sekele SS, Srivastava AK, Trewin B, Villarroel C, Vincent L, Zhai P, Zhang X, Kitching S. 2013. Updated analyses of temperature and precipitation extreme indices since the beginning of the twentieth century: the HadEX2 dataset. Journal of Geophysical Research: Atmospheres, 118(5): 2098–2118. https://doi.org/10.1002/jgrd.50150

Dowle M, Srinivasan A. 2023. data.table: Extension of 'data.frame'. R package version 1.14.8. https://CRAN.R-project.org/package=data.table

Fischer EM, Knutti R. 2015. Anthropogenic contribution to global occurrence of heavy-precipitation and high-temperature extremes. Nature Climate Change, 5(6): 560–564. https://doi.org/10.1038/nclimate2617

Grolemund G, Wickham H. 2011. Dates and times made easy with lubridate. Journal of Statistical Software, 40(3): 1–25. https://doi.org/10.18637/jss.v040.i03

Indian Council of Agricultural Research (ICAR), 1989. Agro-climatic Zone-wise Research and Development Plan for Agriculture. ICAR, New Delhi.

IPCC. 2021. Climate Change 2021: The Physical Science Basis. Contribution of Working Group I to the Sixth Assessment Report of the Intergovernmental Panel on Climate Change. Cambridge University Press: Cambridge. https://doi.org/10.1017/9781009157896

Jain SK, Kumar V, Saharia M. 2013. Analysis of rainfall and temperature trends in northeast India. International Journal of Climatology, 33(4): 968–978. https://doi.org/10.1002/joc.3483

Jones PD, Hulme M. 1996. Calculating regional climatic time series for temperature and precipitation: methods and illustrations. International Journal of Climatology, 16(4): 361–377. https://doi.org/10.1002/(SICI)1097-0088(199604)16:4<361::AID-JOC53>3.0.CO;2-F

Kashyapi AK, Das DK, Sharma AR. 2010. Crop specific requirement of growing degree days and agrometeorological indices in rice growing zones. Mausam, 61(4): 569–578. https://doi.org/10.54302/mausam.v61i4.915

Kaur V, Singh SP, Kingra PK, Singh J. 2024. Climate change impact assessment of growing degree days and thermal growing period of cotton in north-west India. *Journal of Water and Climate Change* **15**: 4731–4744. https://doi.org/10.2166/wcc.2024.288

Kendall MG. 1975. Rank Correlation Methods, 4th edn. Charles Griffin: London.

Kingra PK, Misra AK. 2021. Agricultural input use efficiency and climate change: ways to improve the environment and food security. In: Srivastava AK, Chandra P (eds) Input Use Efficiency for Food and Environmental Security. Springer: Singapore, 33–67. https://doi.org/10.1007/978-981-16-5199-1_2

Kothawale DR, Munot AA, Krishna Kumar K. 2010. Surface air temperature variability over India during 1901–2007, and its association with ENSO. Climate Research, 42(2): 89–104. https://doi.org/10.3354/cr00857

Kumar, P, Kumar, S, Hooda, VS, Neelam, Kumar,A Thakral, SK, Kumar, S, Kumar, P, 2022. Agrometeorological indices influenced by different sowing dates, irrigation and fertilizer levels under late sown Indian mustard in western Haryana. Journal of Agrometeorology 24, 172–178. https://doi.org/10.54386/jam.v24i2.1120

Mann, HB, 1945. Nonparametric tests against trend. *Econometrica* 13(3), 245–259. https://doi.org/10.2307/1907187

McLeod AI. 2022. Kendall: Kendall Rank Correlation and Mann-Kendall Trend Test. R package version 2.2.1. https://CRAN.R-project.org/package=Kendall

Ministry of Agriculture and Farmers Welfare. 2023. Agricultural Statistics at a Glance 2022. Directorate of Economics and Statistics, Government of India: New Delhi. https://agriwelfare.gov.in/Documents/CWWGDATA/Agricultural_Statistics_at_a_Glance_2022_0.pdf

Mishra AK, Tripathi P, Mishra SR, Kumar R. 2007. Heat unit requirement of wheat cultivars as affected by moisture application frequencies. Journal of Agrometeorology, 9(2): 295–298. https://doi.org/10.54386/jam.v9i2.1147

Misra AK, Pandey V, Mishra SK, Yadav SB, Patel HR. 2019a. Growth, phenology and yield modeling for wheat-fallow cropping system in Gujarat. Indian Journal of Agricultural Sciences, 89(8): 1278–1281. https://doi.org/10.56093/ijas.v89i8.92845

Misra AK, Yadav SB, Mishra SK, Tripathi MK. 2019b. Impact of meteorological variables and climate change on plant diseases. In: Kumar, P, Tiwari, AK, Kamle, M, Abbas, Z, Singh, P, (eds) Plant Pathogen: Detection and Management in Sustainable Agriculture. Apple Academic Press, Canada, 313–327. https://doi.org/10.1201/9780429057212-18

Mohan M, Kandya A. 2015. Impact of urbanization and land-use/land-cover change on diurnal temperature range: a case study of tropical urban airshed of India. Science of the Total Environment, 506–507: 453–465. https://doi.org/10.1016/j.scitotenv.2014.11.006

Open Government Data Platform India (OGD). 2022. Boundaries of Agro-Climatic Regions [Dataset]. Ministry of Electronics and Information Technology, Government of India. https://www.data.gov.in/resource/boundaries-agro-climatic-regions

Pal RK, Tripathi P, Mishra AK. 2008. Simulation modeling of growth parameters of wheat genotype using CERES wheat model. Journal of Agrometeorology, 10(Special Issue, Part I): 125–126.

Pandey V, Misra AK, Yadav SB. 2017. Climate change and variability and their impacts on different crops in Gujarat. In: Belavadi, VV, Nataraja, Karaba, NN, Gangadharappa, NR (eds) *Agriculture under Climate Change: Threats, Strategies and Policies*. Allied Publishers: New Delhi, 29–33. ISBN : 9385926373

Pandey V, Misra AK, Yadav SB. 2019. Impact of El Niño and La Niña on Indian climate and crop production. In: Sheraz Mahdi S (ed) Climate Change and Agriculture in India: Impact and Adaptation. Springer International Publishing: Cham, 11–20. https://doi.org/10.1007/978-3-319-90086-5_2

Pebesma E. 2018. Simple features for R: standardized support for spatial vector data. The R Journal, 10(1): 439–446. https://doi.org/10.32614/RJ-2018-009

Perkins-Kirkpatrick SE, Gibson PB. 2017. Changes in regional heatwave characteristics as a function of increasing global temperature. Scientific Reports, 7: 12256. https://doi.org/10.1038/s41598-017-12520-2

Perkins-Kirkpatrick SE, Lewis SC. 2020. Increasing trends in regional heatwaves. Nature Communications, 11: 3357. https://doi.org/10.1038/s41467-020-16970-7

Peterson TC, Folland C, Gruza G, Hogg W, Mokssit A, Plummer N. 2001. Report on the Activities of the Working Group on Climate Change Detection and Related Rapporteurs 1998–2001. WMO/TD-No. 1071. World Meteorological Organization: Geneva. https://etccdi.pacificclimate.org/docs/wgccd.2001.pdf

Planning Commission. 1989. Agro-climatic Regional Planning: An Overview. Planning Commission, Government of India: New Delhi.

Pohlert T. 2023. trend: Non-parametric Trend Tests and Change-point Detection. R package version 1.1.4. https://CRAN.R-project.org/package=trend

Qayoom, S., Mushtaq, N., Kumar, R., Ahmad, L., Lone, B.A., Singh, P., 2022. Pheno-thermal response of exotic high-density apple varieties under temperate conditions of Kashmir. Journal of Agrometeorology 24, 152–156. https://doi.org/10.54386/jam.v24i2.1557

R Core Team. 2023. R: A Language and Environment for Statistical Computing. R Foundation for Statistical Computing: Vienna. https://www.R-project.org/

Rajeevan M, Rohini P, Nair SA, Tirkey S, Goswami T, Kumar N. 2023. Heat and Cold Waves in India: Processes and Predictability. IMD Meteorological Monograph MoES/IMD/Synoptic Met/01(2023)/28. India Meteorological Department, Ministry of Earth Sciences, Government of India: New Delhi. https://imdpune.gov.in/reports.php

Raymond C, Matthews T, Horton RM. 2020. The emergence of heat and humidity too severe for human tolerance. Science Advances, 6(19): eaaw1838. https://doi.org/10.1126/sciadv.aaw1838

Revadekar JV, Kothawale DR, Patwardhan SK, Bhaskar DV, Kumar KK, Khole M, Kumar MRR. 2012. About the observed and future changes in temperature extremes over India. Natural Hazards, 60(3): 1133–1155. https://doi.org/10.1007/s11069-011-9895-4

Rohini P, Rajeevan M, Mukhopadhyay P. 2019. Future projections of heat waves over India from CMIP5 models. Climate Dynamics, 53(1–2): 975–988. https://doi.org/10.1007/s00382-019-04700-9

Rohini P, Rajeevan M, Srivastava AK. 2016. On the variability and increasing trends of heat waves over India. Scientific Reports, 6: 26153. https://doi.org/10.1038/srep26153

Schauberger P, Walker A. 2023. openxlsx: Read, Write and Edit xlsx Files. R package version 4.2.5.2. https://CRAN.R-project.org/package=openxlsx

Sen PK. 1968. Estimates of the regression coefficient based on Kendall's tau. Journal of the American Statistical Association, 63(324): 1379–1389. https://doi.org/10.1080/01621459.1968.10480934

Singh P, Boote KJ, Yogeswara Rao A, Iruthayaraj MR, Sheikh AM, Hundal SS, Narang RS, Singh P. 1994. Evaluation of the groundnut model PNUTGRO for crop response to water availability, sowing dates, and seasons. Field Crops Research, 39(3): 147–162. https://doi.org/10.1016/0378-4290(94)90011-6

Srivastava AK, Rajeevan M, Kshirsagar SR. 2009. Development of a high resolution daily gridded temperature data set (1969–2005) for the Indian region. *Atmospheric Science Letters*, 10(4): 249–254. https://doi.org/10.1002/asl.232

Thiery W, Visser AJ, Fischer EM, Hauser M, Hirsch AL, Lawrence DM, Lejeune Q, Davin EL, Seneviratne SI. 2020. Warming of hot extremes alleviated by expanding irrigation. *Nature Communications*, 11: 290. https://doi.org/10.1038/s41467-019-14075-4

World Meteorological Organization (WMO). 2023. *WMO Climpact: Indices for Climate Extremes*. WMO: Geneva. https://climpact-sci.org

World Meteorological Organization (WMO). 2024. *State of the Global Climate 2023*. WMO-No. 1347. WMO: Geneva. https://library.wmo.int/idurl/4/68835

Yue S, Wang C. 2004. The Mann-Kendall test modified by effective sample size to detect trend in serially correlated hydrological series. *Water Resources Management*, 18(3): 201–218. https://doi.org/10.1023/B:WARM.0000043140.61082.60

Zeileis A, Grothendieck G. 2005. zoo: S3 infrastructure for regular and irregular time series. *Journal of Statistical Software*, 14(6): 1–27. https://doi.org/10.18637/jss.v014.i06

Zhang X, Alexander L, Hegerl GC, Jones P, Klein Tank A, Peterson TC, Trewin B, Zwiers FW. 2011. Indices for monitoring changes in extremes based on daily temperature and precipitation data. *Wiley Interdisciplinary Reviews: Climate Change*, 2(6): 851–870. https://doi.org/10.1002/wcc.147

Zhang X, Hegerl G, Zwiers FW, Kenyon J. 2005. Avoiding inhomogeneity in percentile-based indices of temperature extremes. *Journal of Climate*, 18(11): 1641–1651. https://doi.org/10.1175/JCLI3366.1